International Journal of Rock Mechanics & Mining Sciences 128 (2020) 104262

Contents lists available at ScienceDirect

International Journal of Rock Mechanics and Mining Sciences

journal homepage: http://www.elsevier.com/locate/ijrmms

Airflow disturbance induced by coal mine outburst shock waves: A case study of a gas outburst disaster in China

Aitao Zhou [a,b,c], Meng Zhang [a], Kai Wang [a,*], Derek Elsworth [c], Jiawen Wang [a], Lingpeng Fan [a]

[a] College of Emergency Management and Safety Engineering, China University of Mining and Technology (Beijing), Beijing, 100083, China
[b] State and Local Joint Engineering Laboratory for Gas Drainage & Ground Control of Deep Mines, Henan Polytechnic University, China
[c] Department of Energy and Mineral Engineering, EMS Energy Institute and G3 Center, Pennsylvania State University, University Park, PA, USA

ARTICLE INFO

Keywords:
Coal and gas outburst
Airflow disturbance
Multi-scale coupling model
Shock wave attenuation

ABSTRACT

We explore the magnitude of airflow disturbance in mine roadways induced by gas outburst shock waves. Outburst shock wave propagation in the near-field of the outburst source is established and simulated in three dimensions using FLUENT. The effects in connected but distal roadways are represented by a simplified one-dimensional network model and solved by Flowmaster. A Mesh-based Parallel Code Coupling Interface (MPCCI) is applied to couple the three-dimensional (near source) model and the one-dimensional (distal) model. The coupled model is verified by theoretical analysis and against observations from a coal and gas outburst incident comprising 2887 tonnes of coal that occurred in the Jiulishan coal mine, China and general characteristics of outburst events explored. Simulations demonstrate that airflow disturbance induced by outburst shock waves in the coal mine is principally controlled by the shock wave overpressure and fan pressure provided by the main fan. Of these, the shock wave overpressure exerts the dominant impact. The larger the shock-wave overpressure, the more rapid the decrease of airflow in the roadway branches and the larger the ultimate airflow decrease. Furthermore, the arrival time of the minimum air flow rate is delayed. When the fan pressure is large, the ability to resist airflow disturbance is enhanced and the area subject to countercurrent flow is reduced. The initial air flow rate and the restored air flow rate show less correlation with the shock wave overpressures. However, they are both significantly affected by the pressure of the main fan. This work presents a novel approach for the study of airflow disturbance in underground ventilation networks in coal mines caused by coal and gas outbursts and provides guidance for the design of outburst prevention facilities.

1. Introduction

Airflow at the mining face and in the roadways of underground mines can be severely disrupted during coal and gas outbursts and may trigger secondary disasters, such as gas explosions,[1–3] requiring that these impacts be defined.[4–6] Normal ventilation airflow can be disrupted by the shock waves generated by coal and gas outbursts, potentially generating countercurrents in the far-field,[7,8] with the potential for suffocating flows and gas explosions. Studies have explored outburst mechanisms and preventive measures, *via* a variety of theoretical models.[9–12] These have defined attenuation relations for shock wave attenuation in the near-field of the outburst source. However, understanding of the attenuation of shock wave propagation in the far-field, distant from the outburst source, remains poorly defined. No effective method is available to study the influence of outbursts on underground airflow. An outburst shock wave is known to result from the ejection of a large amount of pulverized coal carried by gas.[13,14] The inertia of the pulverized coal is significant, with particle-particle collisions consuming considerable energy and influencing transport. Thus, the role of inertia in the propagation of shock airflows cannot be neglected in the near-field of the outburst source.[15–17] However, after the outburst shock wave has propagated far from the outburst source, the pulverized coal will gradually settle as the turbulence weakens then abates.[18–20] The pressure gradients for the shock waves vary principally in the propagation direction as do the changes overpressures – enabling transverse gradients to be ignored and allowing the system to be represented by a 1D model.[21] Therefore, the propagation of the outburst shock waves in the near-field and far-field can be decoupled, and calculated separately. A 3D model is needed to simulate the complex propagation characteristics of the shock wave in the near-field, with a 1D model sufficient to

* Corresponding author. College of Emergency Management and Safety Engineering, China University of Mining & Technology (Beijing), Beijing, 100083, China.
E-mail address: safety226@126.com (K. Wang).

https://doi.org/10.1016/j.ijrmms.2020.104262
Received 6 June 2019; Received in revised form 17 January 2020; Accepted 16 February 2020
Available online 19 February 2020
1365-1609/

represent attenuation in the far-field. Thus, the airflow disturbance in the entire underground mine ventilation network can be obtained through the coupling between the 3D and the 1D models. The following establishes a multi-scale coupling model of the propagation characteristics of the outburst shock wave. The model is verified against the case of an outburst at the Jiulishan coal mine, Jiaozuo, China and general characteristics of outburst events explored. This coupling model enables the feasible range of outcomes of outbursts to be explored, providing guidance for mitigation and to inform disaster rescue. In addition, the attenuated shock wave and the delineated region for countercurrent flow provide the basis for the design (resilience and location) of outburst prevention facilities together with locations for the siting of outburst prevention and flow dampers.

2. Multi-scale coupling model for the propagation of outburst shock waves

The different spatial-dimensionalities and processes in the near-field outburst zone (3D-inertia-dominated) and subsequent transport in the mine roadways (1D) enable considerable savings in computation over full 3D representation. The following separately develops an inertia-dominated model for the 3D representation of the outburst zone and a 1D model for mine roadways that are linked via a coupling routine.

2.1. 3D model for shock wave attenuation in the near-field

Outburst shock waves are formed when the air within the roadway is compressed by a high-pressure gas flow.[22,23] Based on conservation of mass, momentum, energy, and mixture components, the governing equations for the outbursts shock wave are:[24]

$$\left.\begin{aligned}
&\frac{\partial \rho}{\partial t}+\frac{\partial \rho u_i}{\partial x_i}=0\\
&\frac{\partial \rho u_i}{\partial t}+\frac{\partial \rho u_i u_j}{\partial x_j}=-\frac{\partial P}{\partial x_i}+\frac{\partial \tau_{ij}}{\partial x_j}\\
&\frac{\partial E_t}{\partial t}+\frac{\partial E_t u_j}{\partial x_j}=-\frac{\partial}{\partial x_j}\left[(P-\tau_{ij})u_i+\tau_{ij}u_j+q_j\right]\\
&\frac{\partial C}{\partial t}+\frac{\partial C u_j}{\partial x_j}=\frac{\partial J_{xj}}{\partial x_j}
\end{aligned}\right\} \quad (1)$$

where $\tau_{ij}=\mu\left[\left(\frac{\partial u_i}{\partial x_j}+\frac{\partial u_j}{\partial x_i}\right)-\frac{2}{3}\delta_{ij}\frac{\partial u_i}{\partial x_i}\right]$; $q_j=-K\frac{\partial T}{\partial x_j}$; $E_t=\rho\left(C_V T+\frac{1}{2}u_i u_i\right)$; $J_{xj}=\Gamma\frac{\partial C}{\partial x_j}$;$C$ represents the gas concentration; C_V represents the specific heat capacity at constant volume; E_t represents the total energy of the gas flow; J_{xj} represents the gas diffusion flow in the j direction; K represents the thermal conductivity of the gas flow; P represents the pressure of the mixed gas; q_j represents the airflow transporting heat in the j direction; t represents time; T represents temperature; u_i represents the average velocity of the airflow in the i direction; u_j represents the average velocity of the airflow in the j direction; ρ represents the density of the gas; μ represents dynamic viscosity of the gas; Γ represents the convection diffusion coefficient of the gas; τ_{ij} represents the shear stress tensor; and δ_{ij} represents the Dirac delta function.

The equations also require a state equation for the solution, here supplied by the ideal gas law. FLUENT is utilized to evaluate the characteristics of the two-phase gas-solid outburst flows in the near-field roadways.

The ideal mixture assumption is that the parameters of the high-pressure mixed flow of gas and pulverized coal in the outburst region (the outburst chamber) are evenly distributed when the outburst reaches the critical state (Fig. 1).

At the critical outburst state, the initial conditions of the high-pressure gas in the outburst chamber are:

$$P_1{=}P \text{ MPa},\ u_1=0,\ T_1=300 \text{ K},\ V=5\%\ (t=0;\ 0<x<\text{L}) \quad (2)$$

where P_1 is the gas pressure in the outburst chamber, MPa; u_1 is the flow velocity, m/s; T_1 is the temperature, K; and V is the volume fraction of pulverized coal in the outburst chamber. The outburst chamber is charged with high-pressure gas as the outburst energy source.

At the critical state of the outburst, the initial properties of the air in the roadway are:

$$P_0=0.1 \text{ MPa},\ u_0=0,\ T_0=300 \text{ K},\ C_0=0\ (t=0;\ x>\text{L}) \quad (3)$$

where C_0 is the gas concentration in the roadway.

2.2. 1D network model for shock wave propagation in the far-field

The propagation of the outburst shock wave far from the outburst source may be simplified from the full three-dimensional simulation in FLUENT into a one-dimensional form. The Flowmaster code is adopted for these 1D flows, and significantly shortens the numerical solution time. In Flowmaster, the compressed high-speed airflow is considered as one-dimensional transient compressible inviscid flow.

Flowmaster comprises a variety of modeling components and is able to simulate the propagation of the outburst shock wave in a one-dimensional pipeline. Typical components are shown in Fig. 2.

The overpressure gradient of the shock wave is typically small, enabling 1D linearization to be applied to each branch of a roadway far from the outburst source. Accordingly, a 1D mine ventilation network model is established using pipeline, flow source, pressure source, corner and loss elements together with other components provided in Flowmaster. These separately represent the underground roadway, outburst source, pressure source, corner roadway, and other structures.

2.3. Multi-scale coupling between outburst (3D) and roadway propagation (1D) models

The propagation and attenuation of the outburst shock wave near the source is represented by FLUENT in 3D with the 1D Flowmaster pipe network model representing the branching roadways in the far-field. These two codes are linked by a multi-scale coupling platform referred to as the Mesh-based Parallel Code Coupling Interface (MPCCI). This enables the ensemble numerical analysis of the complete propagation process of the outburst shock wave to be followed throughout the entire underground roadway network.

The multi-scale coupling referred to in this paper is the coupling between the FLUENT and Flowmaster codes. The exchange of pressure

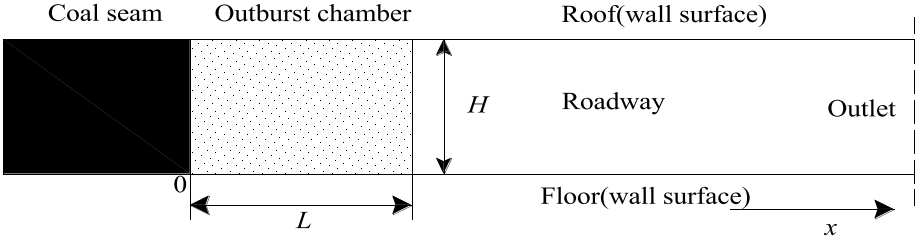

Fig. 1. Geometric model of an outburst in a straight roadway.

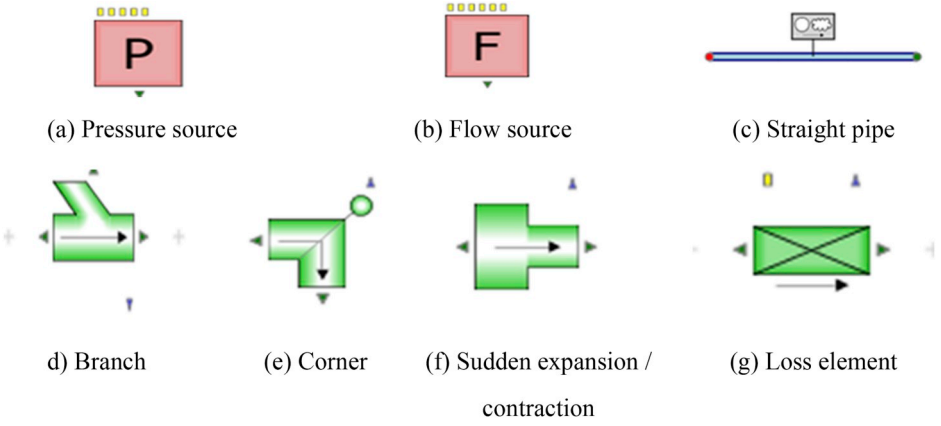

Fig. 2. Schematic of components in the Flowmaster code.

magnitudes and mass flow rates in transient coupling may be taken as an example. Nodal flows and nodal pressures are defined in the 1D calculation with the opening divided into *n* nodes in the 3D model. Each node corresponds to a surface element to constitute the overall surface of the unit. The essence of parameter exchange is to make the flow and pressure of the one-dimensional node consistent with the total flow and

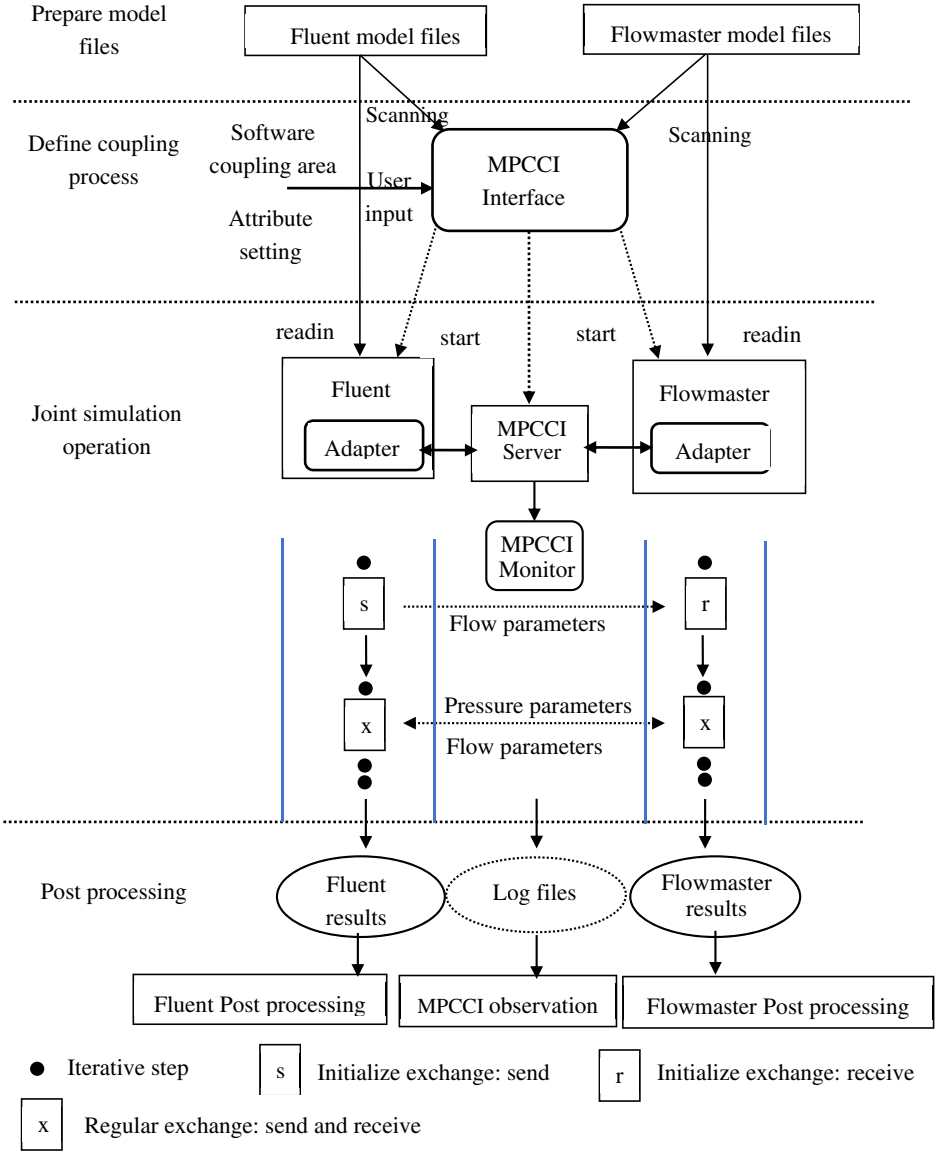

Fig. 3. Procedures for coupling the Flowmaster and FLUENT codes.

surface pressure of the unit. In the transient initialization exchange, FLUENT first sends the flow parameters to the Flowmaster code. The two codes then operate in parallel and perform regular parameter exchanges after each iteration step. FLUENT sends the flow parameters to the Flowmaster code, and the Flowmaster code returns the pressure parameters to FLUENT until both data sets finally reach convergence. The specific coupling steps are shown in Fig. 3.

3. Case study of shock wave attenuation and airflow disturbance

Coal and gas outburst accidents occur frequently in Chinese coal mines and are extremely harmful. For the conditions of one specific and well documented gas outburst incident we apply this model as a verification exercise. We then apply the coupled simulation model to explore controls on shock wave attenuation and airflow disturbance in other generic mine geometries.

3.1. Overview of outburst

A serious outburst accident occurred at the Jiulishan coal mine, Jiaozuo, Henan province, China early in the morning of August 23, 2005.[25] The volume of the ejected gas at heading face 15051 was 279, 000 m^3, the mass of outburst coal was 2887.15 t, and the maximum airflow reversal reach was more than 800 m. The total intake air flow rate was 12,643 m^3/min and the total return air flow rate was 13,103 m^3/min under normal production conditions in the mine. The principal mining faces were: working face 15011 and heading faces 15051, 15071 and 15061. A 2 × 15 kW auxiliary fan was utilized at heading face 15051 for air supply of 356 m^3/min to counter the maximum gas emission rate of 2.7 m^3/min present during normal mining. The fresh air flow rate at working face 15061 was 20.71 m^3/s.

A simplified ventilation network for the mining area in the Jiulishan coal mine is shown in Fig. 4. The outburst occurred at the heading face (15051) and principally affected the area between nodes 3 and 8 in the network model. Branches 17, 18 and 19 are the most readily influenced by the outburst shock wave, and branches 9 and 14 may also be involved. In addition, branches 10 and 12 (the air-return entry at heading face 15061 and at working face 15011) were also r disturbed.

A diagram of the outburst-disturbed area in the mine is simplified by selecting the major branches between nodes 3 and 8 in the ventilation network based on heading face 15051, shown in Fig. 5.

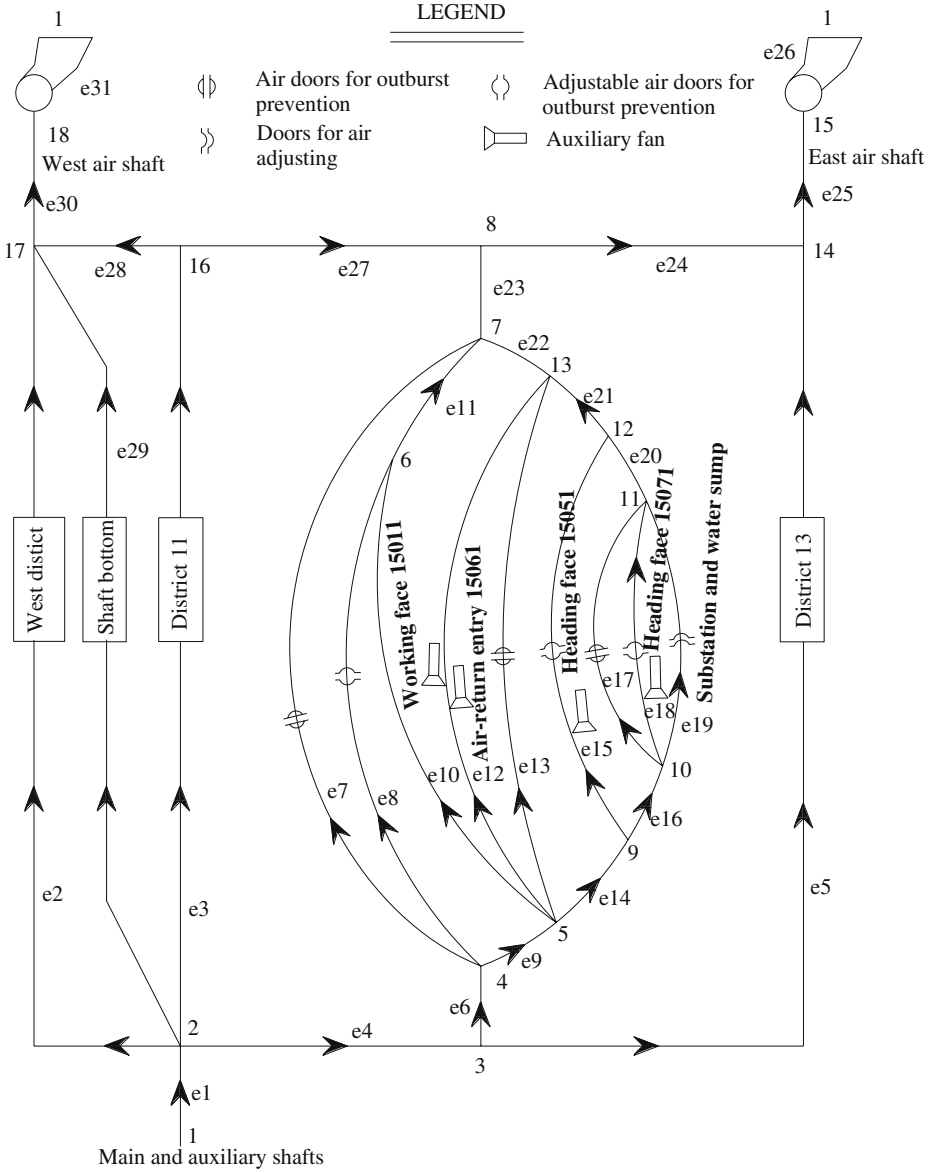

Fig. 4. Ventilation network diagram for the Jiulishan coal mine.

3.2. Analysis of outburst shock airflows

The outburst is driven by the initial stored energy and consumed by the general overpressure of the shock wave.

(1) The initial energy of outburst shock airflow

The initial energy of the outburst shock airflow comprises the elastic energy of the coal and gas expansion energy. The calculations for the initial energy of outburst shock airflows are:

① Elastic energy of coal

The elastic energy of the coal body is an important part of the initial energy for the shock airflow. When calculating the elastic energy of the coal, not only the self-weight stress of the coal body but also the stress applied to the coal should be considered. According to the characteristics of the Jiulishan mining area, the stress concentration factor is of the order of ~2. The depth of the working face (15051) is 416 m. The principal stresses in the three directions are taken as:

$$\sigma_1 = \sigma_2 = \sigma_3 = 2 \times 0.025 \times 416 = 20.8Mpa \tag{4}$$

According to measurements of the mechanical properties of coal samples taken from the outburst area, the elastic modulus E is 280 MPa, the Poisson ratio μ is 0.3, and the bulk density γ is 1.54 t/m^3. Thus the elastic energy of coal per tonne is:

$$W_1 = \frac{1}{2E}\left(3\sigma_1^2 - 2\mu \times 3\sigma_1^2\right) \Big/ 1.54 = 0.602 \ \ \mathrm{MJ/t} \tag{5}$$

② Expansion energy of free gas per tonne of coal

From the analysis of most outburst cases, the entire outburst process is largely adiabatic, and the adiabatic coefficient n is approximately 1.25. In general, V_{free} is ~10% of the gas content in the coal seam. The measured gas content in the air-return entry at working face 15051 is 22.05 m^3/t, and the gas pressure is 0.86 MPa. Thus, the expansion energy of free gas per tonne of coal is:

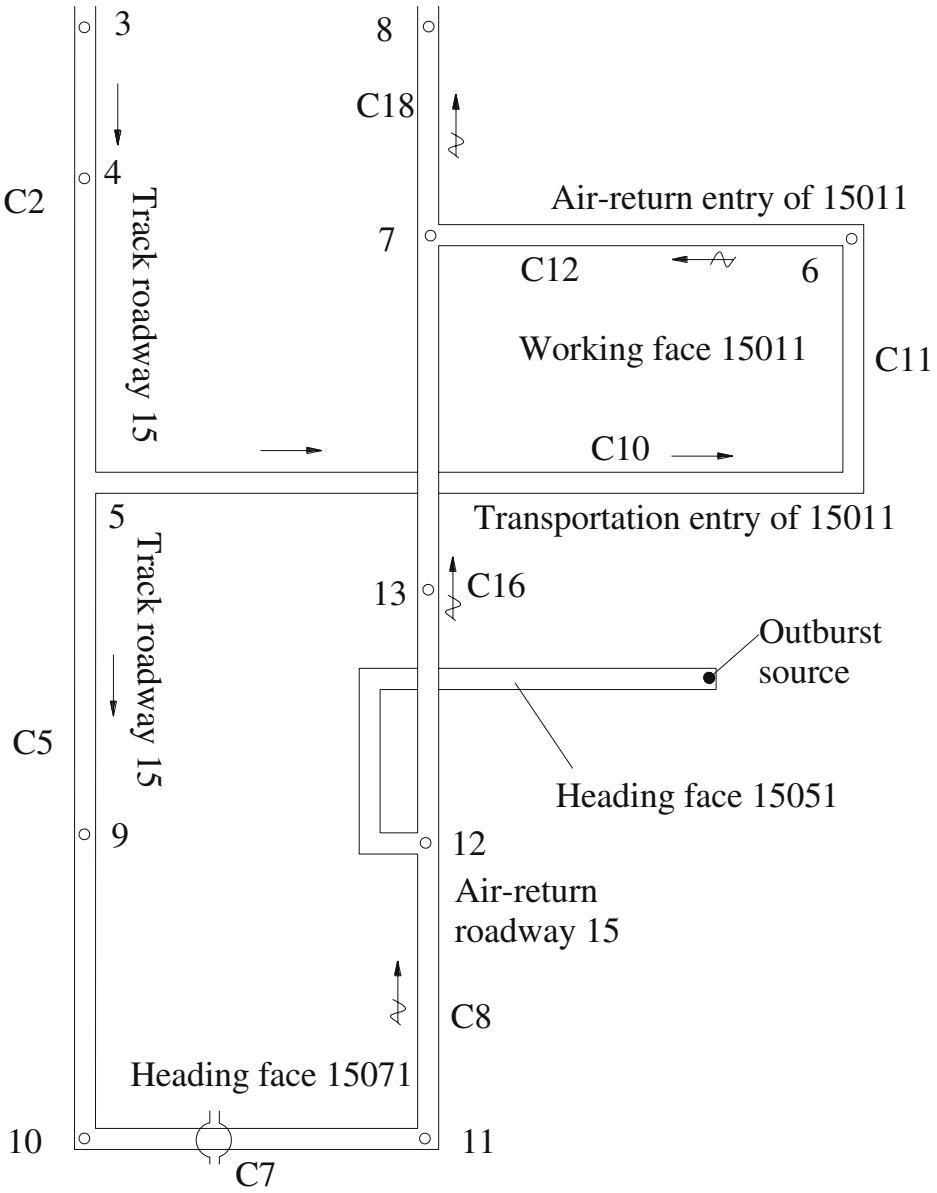

Fig. 5. Simplified diagram of the area disturbed by the outburst shock wave in the Jiulishan mine.

$$W_{21}=\frac{P_0V_{free}}{n-1}\left[\left(\frac{P_c}{P_0}\right)^{\frac{n-1}{n}}-1\right]=\frac{22.05\times0.1\times0.1}{1.25-1}\left[\left(\frac{0.86}{0.1}\right)^{\frac{1.25-1}{1.25}}-1\right]=0.476\ \text{MJ/t} \tag{6}$$

③ Expansion energy per tonne of coal induced by gas desorption

The gas content coefficient α is 3.16 $m^3/(t{\cdot}MPa^{0.5})$. The original ambient pressure P_0 in the outburst region is 0.1 MPa, and the gas pressure P_c in the coal seam before the outburst is 0.86 MPa. The original ambient temperature T_0 in the outburst roadway is 293 K. Then the expansion energy per tonne of coal induced by gas desorption is:

$$W_{22}=\frac{RT_0\alpha}{22.4(n-1)}\left\{\left[\frac{n}{3n-2}\left(\frac{P_c}{P_0}\right)^{\frac{n-1}{n}}-1\right]\sqrt{P_c}+\frac{2(n-1)}{3n-1}\sqrt{P_0}\right\}=0.239\ \text{MJ/t} \tag{7}$$

④ Total initial outburst energy per tonne of coal

The calculations show that the elastic energy of the coal mass per tonne W_1 is 0.602 MJ/t; the expansion energy of free gas per tonne of coal W_{21} is 0.476 MJ/t; the expansion energy of gas desorption per tonne of coal W_{22} is 0.239 MJ/t. This contributes a total initial outburst energy per tonne of coal is:

$$W=W_1+W_{21}+W_{22}=1.317\ \text{MJ/t} \tag{8}$$

The shock airflow both breaks and transports the coal during propagation, consuming the outburst energy. Therefore, the maximum total initial energy of the outburst per tonne of coal is 1.317 MJ.

(2) Overpressure generated by outburst shock airflow in the roadway

The shock airflow comprises a shock wave and related gas flows, with the shock waves generated by the outburst continuously attenuated in the roadway. The attenuation of the outburst shock wave in a straight roadway is described as:

$$P_1=P_0+\frac{2\rho_0D^2}{k+1}\left(1-\frac{c_0^2}{D^2}\right)=P_0+\delta W\Big/(AL) \tag{9}$$

where the roadway cross section A is 8 m^2, and the air compression coefficient k is 1.4, resulting in,

$$\delta=\frac{2(k+1)^2(k-)}{3k-1}=1.44. \tag{10}$$

The gas energy per tonne of coal is 1.317 MJ. Then, the shock wave overpressure ΔP at different locations in the roadway can be expressed as:

$$\Delta P=P-P_0=\frac{\delta W}{AL}=\frac{1.44\times1.317G}{8L}=237.06\frac{G}{L}Pa \tag{11}$$

where G represents the outburst intensity (outburst coal mass).

The measured outburst intensity is 2887.15 t according to the accident investigation, resulting in the shock wave overpressures at different locations in the outburst roadway as shown in Fig. 6.

It can be seen from Fig. 6 that the outburst shock wave overpressure monotonically attenuates with distance from the source. The distance from the outburst source to the working face (15011) is ~600 m, thus the maximum overpressure generated at the intersection of the air-return entry and the air-return roadway (15) is 1141 Pa. Furthermore, the maximum overpressure does not consider the energy consumed in breakage of the coal, nor energy losses around corners and at bifurcating roadways. Therefore, the actual overpressure of the shock wave generated at the intersection of the air-return entry and the air-return roadway (15) must be far lower than 984 Pa. Airflow reversals at the working face are determined by two factors. One is the outburst shock wave overpressure generated at the working face and the second is the ventilation resistance between the inlet and return sections of the working face. Only when the shock wave overpressure is greater than the ventilation resistance of the sections, will the airflows at the working face be reversed. According to the ventilation resistance measured in the Jiulishan coal mine in 2002, the ventilation resistance between the inlet and air-return entries at the working face is 901 Pa. Since the outburst shock wave overpressure generated in this region is less than 901 Pa, an airflow reversal will not occur at the working face.

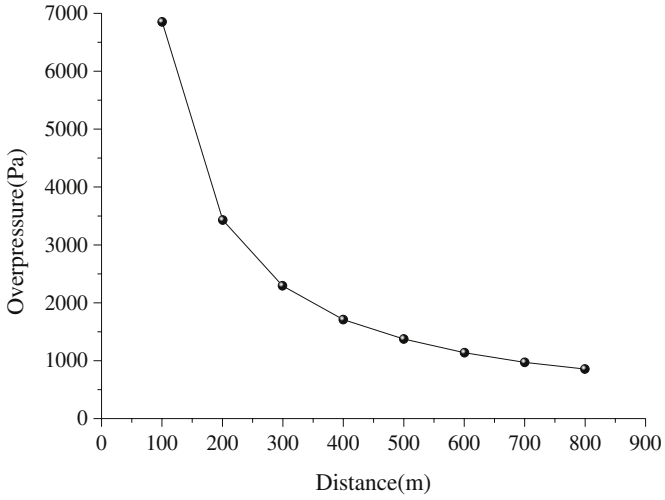

Fig. 6. Variation of shock wave overpressure along a roadway.

3.3. Numerical simulation and analysis

According to Fig. 4, a coupled model for Fig. 5 is established (Fig. 7). The outburst chamber is 6 m long and 2 m high in accordance with the in-situ mining geometry. Since the corner structure at roadway intersections significantly blocks the outburst air flow, an intersection between the heading face and the air-return roadway, 100 m away from the outburst source, is selected as the coupling surface for the outburst zone in the Jiulishan coal mine with the model for near-field response established using FLUENT and that for the far-field using Flowmaster. On the coupling surface, FLUENT sends the flow parameters to the Flowmaster code, and the Flowmaster code returns the pressure parameters. In the initial coupling stage, an insignificant initial flow rate will be given in the Flowmaster code as 0.001 m^3/s.

Based on the mine ventilation parameters measured under normal production conditions, the previous data show that the air flow rate at the working face is 20.71 m^3/s, and the ventilation resistance measured between the supply and the return air entries is 901 Pa.

The ventilation network of the outburst-disturbed area in the Jiulishan coal mine before the outburst is constructed is shown in Fig. 7. According to the field investigation, the total air pressure in the simplified model is 2000 Pa. Additionally, the resistance to airflow and the impact of corners in the roadway is represented by pressure loss elements by adjusting loss coefficients to achieve realistic ventilation parameters. In Fig. 7, numerical simulations show that component C11 represents the working face with an air flow rate of 21 m^3/s. The differential pressure between the intake and return airways at the working face is 910 Pa. The field measured data show that the air flow rate at the working face is 20.71 m^3/s and the ventilation resistance between the intake and the air-return entries is 901 Pa. Therefore, it is concluded that

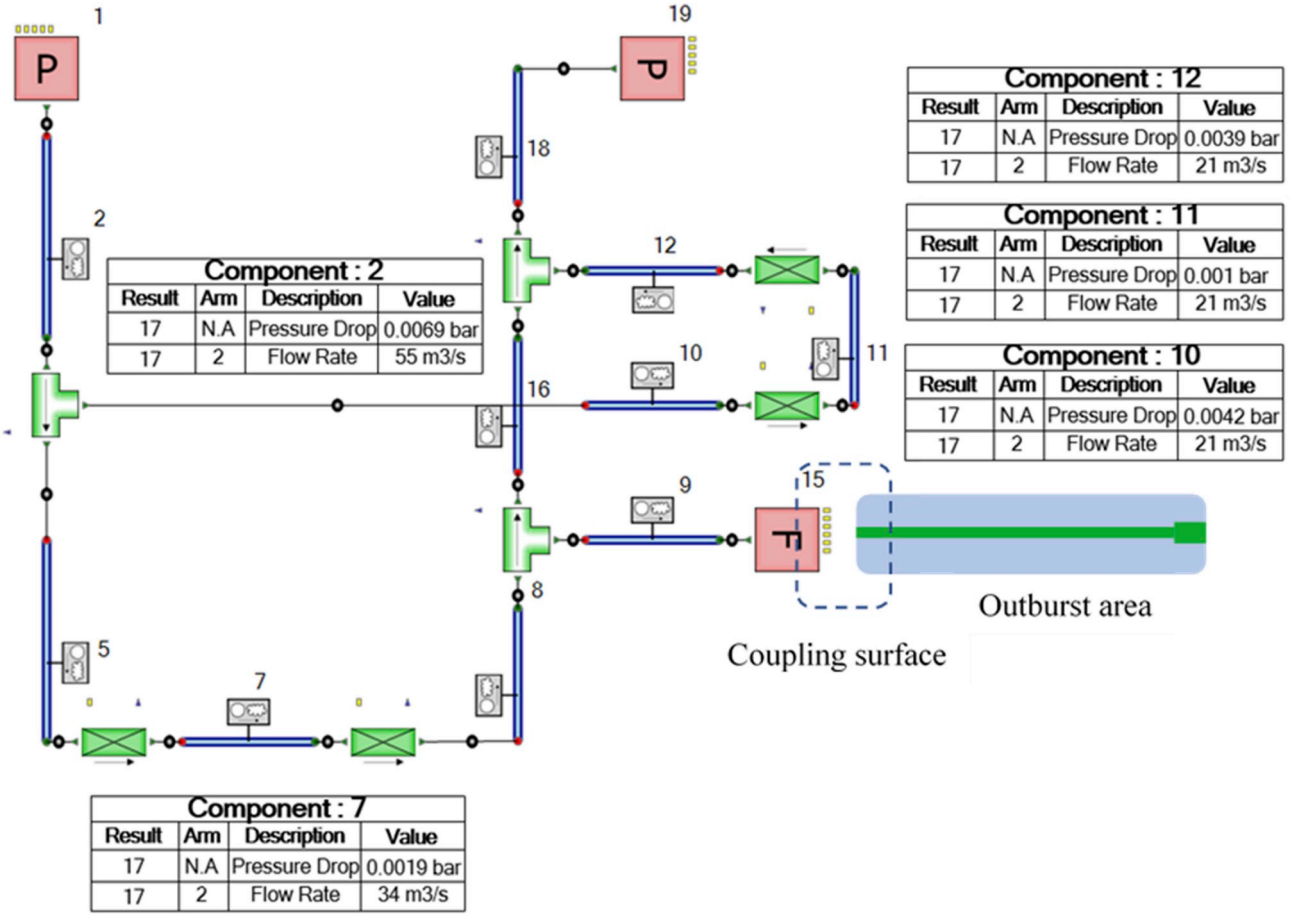

Fig. 7. Coupled model for the outburst-disturbed area in the Jiulishan mine.

the simulated ventilation model is close to the actual ventilation conditions before the outburst.

3.4. Coupled simulations

The relationship between the overpressure of the shock wave and distance from the outburst source is obtained through theoretical representation of the propagation characteristics of the outburst shock wave in the straight roadway (Fig. 6).

As shown in Fig. 6, the overpressure of the outburst shock wave is 7000 Pa at the intersection of the heading face and the air-return roadway (15, which is 100 m away from the outburst source). The factors affecting outburst intensity remain so complex that it is difficult to evaluate them at the outburst source. However, it is feasible to define an equivalent intensity by ensuring that the overpressure at a prescribed location, remote from the outburst source, matches the known history of propagation of the shock wave. The following adopts such an equivalent outburst intensity by adjusting the gas pressure in the outburst chamber *P* to realize a peak overpressure at the monitored surface coupled by MPCCI, is 7000 Pa.

In Fig. 8, the peak pressure monitored at the coupling surface is 7800 Pa – congruent with the overpressure of the outburst. At 0.16s the peak shock wave pressure arrives, passes the air-return roadway (15) and then enters the ventilation network. The specific results are shown in Fig. 9.

In Fig. 9, the temporal and spatial variations of shock wave pressure in vulnerable roadways are shown. It should be noted that the values of pressure derived from Flowmaster are the absolute pressure. The shock wave is divided into two flows after exiting the driving roadway - one propagating against the steady airflow and the other propagating in the

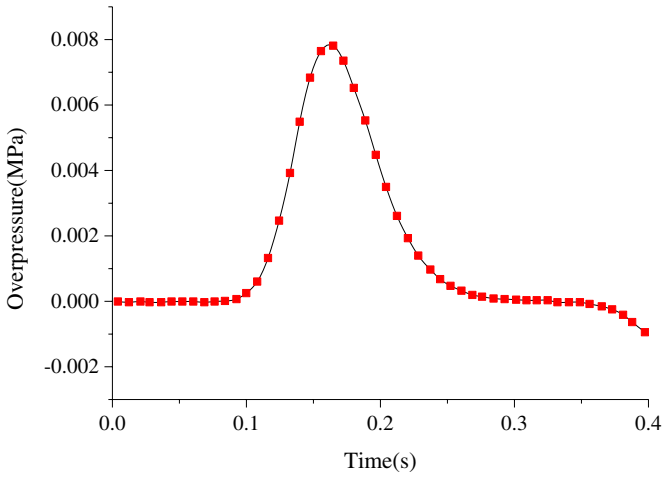

Fig. 8. Variation of overpressure with time at the coupling surface, 100 m away from the outburst source.

airflow direction. Branch C8 represents the lower section of the closest air-return roadway to the outburst source with a length of 170 m. The airflow resistance and propagation attenuation from the coupling surface are small, and the peak overpressure in this roadway is 7500 Pa. Branch C7 represents excavation roadway 15071, with a length of 60 m with the peak overpressure in this roadway decreasing to 5200 Pa. In general, the peak pressures do not change significantly nor does the arrival time of the peak pressure - due to the short length of the roadway.

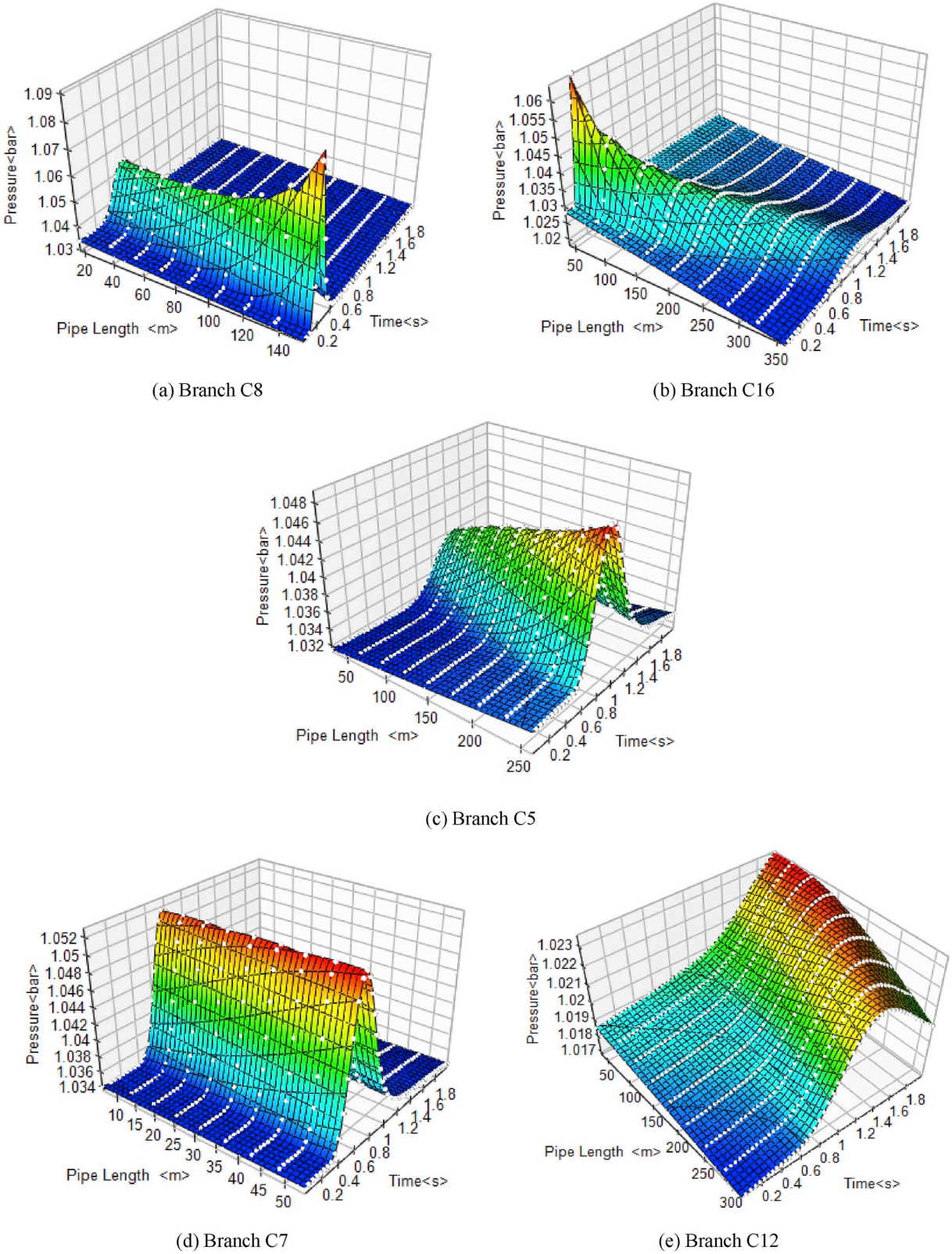

Fig. 9. Surfaces of gas overpressure variation with time and roadway (pipe) length for different roadways.

Branch C5 represents the lower section of the track roadway (15), with a length of 290 m. The peak overpressure has been attenuated to 4600 Pa at the entrance of the roadway. However, for propagation in the direction of the airflow, the shock wave enters the main return airway C18 along the upper section of the air-return roadway C16. This then enters the air-return entry C12 at working face 15011. The overpressure in C16 is attenuated from 6500 Pa to 3500 Pa - much larger than that in C12. The length of C16 is 400 m, with C12 350 m long, and the coupling surface ~100 m away from outburst source. Thus, the end of the air-return entry is more than 800 m away from the source. There the

arrival time of the peak pressure is delayed to 1.8 s or even 2 s after the initiation of the outburst and the overpressure at the rightmost end decreases to 1800 Pa.

The theoretical analysis of overpressure attenuation shows that the peak overpressure is 7000 Pa at 100 m and is attenuated to 1000 Pa at 800 m. The simulation results show that the peak is 7800 Pa at 100 m and is attenuated to 2100 Pa at 800 m. Thus, the peak pressure in the simulations is higher, but the attenuation is slightly smaller than that in the theoretical analysis. This is principally due to the settling and accumulation of the coal particles and a resulting increase in the flow resistance – a feature that is difficult to consider in simulations. Neglecting the presence of solid phase particles in two-phase outburst flows leads to a decrease in the propagation resistance, with an attenuation smaller than in the simulations. In addition, the attenuation caused by roadway structures is also difficult to quantify accurately. The attenuation factors for the roadway structures used in the 1D simulations are also obtained from numerical simulations with FLUENT, with the factors representing roadways of different lengths being appropriately scaled. In general, the peak overpressures and their attenuations are similar and the simulations reliable.

As shown in Fig. 10, when the shock wave enters the air-return roadway (15), the airflow in the roadway is disrupted by the overpressure. The key to the airflow reversal is that the overpressure generated by the outburst shock waves is greater than the ventilation resistance. Influenced by overpressure in the roadways, the air flow rate in branches C2, C5, C7 and C12 decrease to different extents. Branches C2 and C12 are furthest away from the outburst source and the overpressure is insufficiently large to cause a reversal. Therefore, the impacts on these branches are small, and the airflow flow rate is only slightly attenuated. Branch C2 is 620 m away from the outburst source, and C12 is only 500 m away from the outburst source, thus C12 is disturbed earlier.

Different from branches C2 and C12, C5 and C7 both experience a negative air flow rate at 0.54s and 0.75s – resulting in airflow reversals. C7 is closer to the outburst source, thus the reversal occurs earlier. But the countercurrent flow rate is only 6.2m^3/s, and airflow in C12 is not reversed, resulting in only a small outburst shock wave overpressure. This is consistent with the observation that the countercurrent flow region reached more than 600 m.

4. Analysis of outburst shock wave attenuation and airflow disturbance

The coal and gas outburst provides energy for shock wave propagation while the initial ventilation pressure in the mine provides resistance against propagation. The outburst intensity and mine ventilation conditions have a significant influence on shock wave attenuation and the resulting airflow disturbance in the coal mine. We conduct a parametric sensitivity study on the resulting in-mine airflows by setting different shock wave overpressures as the outburst source and fan pressures as the pressure source. However, the factors affecting the overpressure of the shock wave at the outburst source is complex, so we adopt overpressures at the coupling surface 100 m away from the source. The fan pressure is 2000 Pa for an air flow rate of 20 m^3/s, providing an air velocity of 2.8 m/s at the working face under normal production conditions. First, the fan pressure is fixed, and the outburst intensity is changed. The peak overpressure at the coupling surface is successively decremented between 12000 Pa and 6500 Pa. Then the outburst intensity is fixed, and the fan pressure is decremented between 2500 Pa and 1500 Pa. The simulations show that when the overpressure increases to 12000 Pa, countercurrent flow occurs in the air-return entry (15011). The countercurrent flow region extends to more than 800 m. Once the outburst intensity decreases to 6500 Pa, the air in heading face 15071 is almost stagnant, but no countercurrent flow occurs. When the fan pressure decreases to 1500 Pa, the countercurrent flow becomes more significant, and the initial air flow rate and also the restored air flow rate, are both slightly reduced. Air flow rate increases significantly, and airflow is least disrupted by the shock wave when the fan pressure increases to 2500 Pa – in this condition airflow disturbance is greatly resisted. In the comparisons, overpressure attenuation in the various branches is nonintuitive, but airflows change, nonetheless. Sensitive branches C5, C7 and C12 are selected to compare airflow changes under different conditions (Fig. 11).

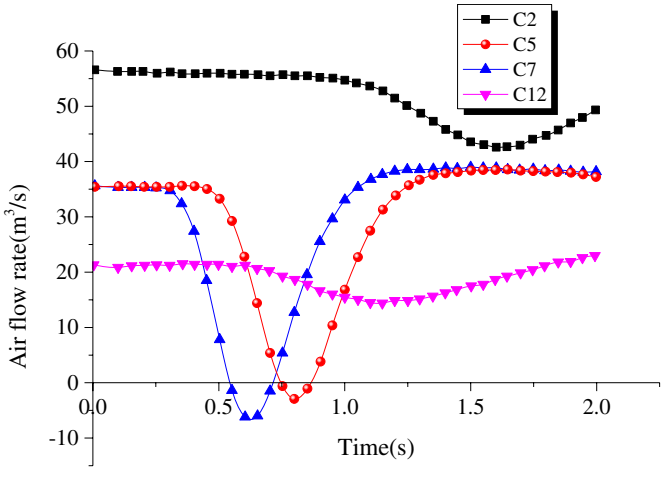

Fig. 10. Variation of airflow with time in key roadways (pipes) during the outburst.

Apparent from Fig. 11 is that airflows are disturbed and in some cases even reversed in the various roadways. In Fig. 11(a), a countercurrent flow occurs in branch C5, namely the track roadway under the original outburst conditions (the overpressure at the coupling surface is 7800 Pa; the fan pressure is 2000 Pa). Once the fan pressure is increased to 2500 Pa, the countercurrent flow disappears from branch C5. The same result is achieved when the shock wave overpressure is reduced to 6500 Pa. If the fan pressure is maintained at 2000 Pa and the shock wave overpressure is increased to 12000 Pa, the countercurrent flow reappears and increases sharply. Similar phenomena are observed in Fig. 11 (b) and (c). However, the arrival time of the minimum air flow rate is delayed with increasing shock wave overpressure. In Fig. 11(c), air-return entry 15011, represented by branch C12, is nearly 800 m away from the outburst source. The change of air flow rate in C12 is small with the fan pressure, but when the shock wave overpressure increases to 12000 Pa, the change in air flow rate is significant with flow reversals also occurring.

Through these comparisons, it is inferred that airflow disturbance in generic mines, and in particular in the reference mine, is principally controlled by the interaction between the shock wave overpressure and fan pressure provided by the main fan. Of these, the shock wave overpressure typically imparts the greater impact. The larger the shock wave overpressure, the faster the air flow rate in the roadway branches decrease and the larger the reduced magnitude. Furthermore, the arrival time of the minimum air flow rate is delayed. When the fan pressure is large, the ability to resist airflow disturbance in the mine ventilation is enhanced and the area subject to countercurrent flow is reduced and ultimately vanishes. Conversely, as the fan pressure is reduced, the air flow supply in the mine is significantly reduced. The initial air flow rate and the restored air flow rate show less correlation with the shock wave overpressures. However, they are both significantly affected by the pressure of the main fan.

5. Conclusions

This study has explored the coupling of 3D near-field and 1D far-field network models to represent the transient shock wave dynamics of coal and gas outbursts. The results have been benchmarked against

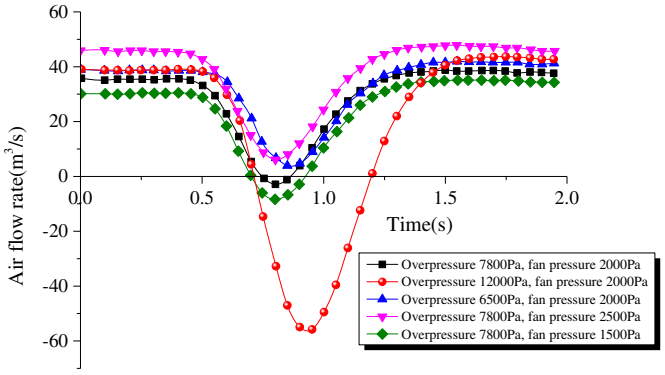

(a) Branch C5

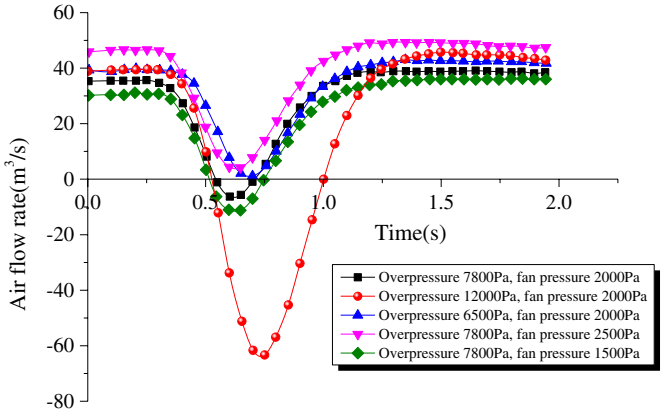

(b)Branch C7

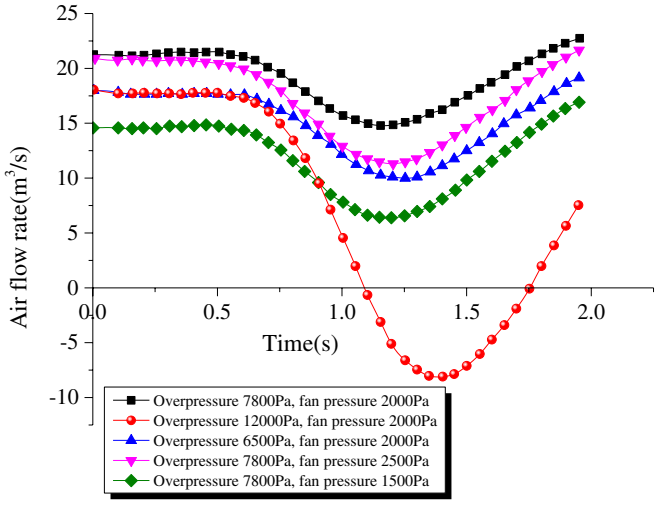

(c) Branch C12

Fig. 11. Comparison of variation in airflow with time in roadways for different conditions.

theoretical solutions with the coupled models linking 3D inertia-dominated response with 1D transport in roadways. The complex coupled model has been benchmarked against a well-documented outburst incident to explore key mechanisms. A parametric study has been conducted for a "generic" mine to understand key impacts and mitigation strategies. The following conclusions are drawn:

(1) Peak overpressures at different locations in the roadway are obtained by using a theoretical representation of outburst shock wave attenuation. We show that the overpressure generated by the outburst shock wave is less than 901 Pa, insufficient to reverse the airflow at the working face (15011) which is consistent with the coupled 3D-1D simulations.

(2) Coupled simulations show that when the peak overpressure on the coupling surface is 7800 Pa, countercurrent flow occurs in parts of the network, specifically in the lower section of the air-return roadway 15, in heading face 15071 and the track roadway, and that the countercurrent flow region reaches more than 600 m from the outburst source. The modeled overpressures, pressure attenuation and regions and velocities of countercurrent flows are in good agreement with the modeled outburst incident.

(3) Airflow disturbance in mines, and in particular in the reference mine, is principally controlled by the shock wave overpressure and fan pressure provided by the main fan. Of these, the shock wave overpressure has the greater impact. The larger the shock wave overpressure, the faster the air flow rate in the roadway branches decrease and the larger the reduced magnitude. When the main fan pressure increases from 2000 Pa to 2500 Pa, the ability to resist airflow disturbance in the mine ventilation is enhanced, and the area subject to countercurrent flow is reduced and ultimately is eliminated. Conversely, as the main fan pressure is reduced to 1500 Pa, the air flow supply in the coal mine is significantly reduced, and countercurrent flow is more likely to occur and over a greater extent in the mine.

(4) The arrival time of the minimum quantity air flow is delayed by 0.5s when the shock wave overpressure increases to 12000 Pa. The initial air flow rate and the restored air flow rate show less correlation with the shock wave overpressures. However, they are both significantly affected by the pressure of the main fan.

Declaration of competing interest

The authors declare no conflict of interest.

Acknowledgments

This research is financially supported by National Natural Science Foundation of China (51774292, 51474219, 51874314, 51604278, 51804312), the Research Fund of State and Local Joint Engineering Laboratory for Gas Drainage & Ground Control of Deep Mines (Henan Polytechnic University), the Yue Qi Distinguished Scholar Project, China University of Mining & Technology, Beijing, the Yue Qi Young Scholar Project, China University of Mining &Technology, Beijing.

Appendix A. Supplementary data

Supplementary data to this article can be found online at https://doi.org/10.1016/j.ijrmms.2020.104262.

References

1 Wang L, Cheng Y, Liu H. An analysis of fatal gas accidents in Chinese coal mines. *Saf Sci*. 2014;62:107–113.
2 Chen H, Qi H, Long R, Zhang M. Research on 10-year tendency of China coal mine accidents and the characteristics of human factors. *Saf Sci*. 2012;50(4):745–750.
3 Wang S, Elsworth D, Liu J. Mechanical behavior of methane infiltrated coal: the roles of gas desorption, stress level and loading rate. *Rock Mech Rock Eng*. 2013;46(5):945–958.
4 Nie W, Liu Y, Li CJ, Xu J. A gas monitoring and control system in a coal and gas outburst laboratory. *J Sensors*. 2014, 172016.
5 Díaz Aguado MB, González Nicieza C. Control and prevention of gas outbursts in coal mines, Riosa–Olloniego coalfield, Spain. *Int J Coal Geol*. 2007;69(4):253–266.
6 Li T, Cai MF, Cai M. A review of mining-induced seismicity in China. *Int J Rock Mech Min*. 2007;44(8):1149–1171.
7 Sun H, Cao J, Li M, et al. Experimental research on the impactive dynamic effect of gas-pulverized coal of coal and gas outburst. *Energies*. 2018;11(4):797.
8 Zhou A, Wang K, Wang J, Feng T. The role of methane buoyancy on the stability of airway airflow in underground coal mine ventilation. *J Loss Prevent Proc*. 2018;54:346–351.
9 Xue S, Wang G, Wang Y, Xie J. A coupled approach to simulate initiation of outbursts of coal and gas — model development. *Int J Coal Geol*. 2011;86:222–230.

10 Xue S, Yuan L, Wang Y, Xie J. Numerical analyses of the major parameters affecting the initiation of outbursts of coal and gas. *Rock Mech Rock Eng*. 2014;47(4):1505–1510.
11 Chen KP. A new mechanistic model for prediction of instantaneous coal outbursts — dedicated to the memory of Prof. Daniel D. Joseph. *Int J Coal Geol*. 2011;87(2):72–79.
12 Xu T, Tang CA, Yang TH, Zhu WC, Liu J. Numerical investigation of coal and gas outbursts in underground collieries. *Int J Rock Mech Min*. 2006;43(6):905–919.
13 Zhu WC, Liu J, Sheng JC, Elsworth D. Analysis of coupled gas flow and deformation process with desorption and Klinkenberg effects in coal seams. *Int J Rock Mech Min*. 2007;44(7):971–980.
14 Guo H, Cheng Y, Ren T, et al. Pulverization characteristics of coal from a strong outburst-prone coal seam and their impact on gas desorption and diffusion properties. *J Nat Gas Sci Eng*. 2016;33:867–878.
15 Chen E, Wang L, Cheng Y, et al. Pulverization characteristics of coal affected by magmatic intrusion and analysis of the abnormal gas desorption index on drill cuttings. *Adsorpt Sci Technol*. 2018;36:805–829.
16 Cao YX, Davis A, Liu RX, Liu XW, Zhang YG. The influence of tectonic deformation on some geochemical properties of coals - a possible indicator of outburst potential. *Int J Coal Geol*. 2003;53(2):69–79.
17 Laslandes S, Sacré C. Transport of particles by a turbulent flow around an obstacle – a numerical and a wind tunnel approach. *J Wind Eng Ind Aerod*. 1998;74:577–587.
18 An F, Cheng Y, Wang L, Li W. A numerical model for outburst including the effect of adsorbed gas on coal deformation and mechanical properties. *Comput Geotech*. 2013;54:222–231.
19 Zhao T, Guo W, Tan Y, Yin Y, Cai L, Pan J. Case studies of rock bursts under complicated geological conditions during multi-seam mining at a depth of 800 m. *Rock Mech Rock Eng*. 2018;51(5):1539–1564.
20 Hu Q, Zhang S, Wen G, Dai L, Wang B. Coal-like material for coal and gas outburst simulation tests. *Int J Rock Mech Min*. 2015;74:151–156.
21 Zhao W, Cheng Y, Guo P, Jin K, Tu Q, Wang H. An analysis of the gas-solid plug flow formation: new insights into the coal failure process during coal and gas outbursts. *Powder Technol*. 2017;305:39–47.
22 Zhang J, Wang K, Wei C. Formation and propagation of shock waves during coal and gas outbursts. *J Min Safety Eng*. 2010;27(1):67–71.
23 Wu A, Jiang C, Tang J. Study on propagation laws of shock wave in coal-rock mass under the effect of gas outburst. *J China Coal Soc*. 2010;35(10):1644–1648.
24 Wang K, Zhou A, Zhang J, Zhang P, Li C. Study of the shock wave propagation and gas flow during a coal and gas outburst at the roadway with a right-angled bend. *J China Univ Min Technol*. 2011;40(6):858–862.
25 Wang K, Zhou A. *The Catastrophic Law of Coal and Gas Outbursts*. Xuzhou: China University of Mining and Technology Press; 2014.